How entraining density currents influence the ocean stratification

A. K. Wåhlin[1] and C. Cenedese[2]

[1]Oslo University
Dept. of Geosciences, Oceanography
PB 1022 Blindern
N- 0315 Oslo
Norway
[2]Woods Hole Oceanographic Institution
Physical Oceanography
MS #21
Woods Hole
MA 02543
USA

Abstract

The sensitivity of the basin-scale ocean stratification to the vertical distribution of plume entrainment is being analyzed. A large ocean basin supplied by dense water from an adjoining marginal sea is considered. The dense water flows into the ocean basin as an entraining density current and interleaves at the bottom (or at the level of neutral density), where it deposits a mixture of marginal sea- and basin water. As the basin water, i.e. 'old' plume water, is entrained and re-circulated in the plume a stratification develops in the basin. The mixture deposited at the bottom hence contains an increasing fraction of marginal sea water, and the basin density increases with depth as well as with time. A stationary solution in which diffusion of buoyancy from above is important is approached asymptotically in time.

Non-diffusive solutions to the initial transient adjustment, as well as the diffusive asymptotic state, have been studied in four different parameterizations of plume entrainment. It is shown that in the transient regime the basin stratification and plume density are highly sensitive to how mixing is parameterized. The stationary diffusive solution that is approached asymptotically in time is less sensitive to parameterization but depends strongly on basin topography, source water density, and buoyancy flux at the surface.

1. Introduction

Marginal seas usually have waters that are cooled (high-latitude) or evaporated, hence dense water is formed by either being cooler or saltier than the surrounding oceans. The dense water can then flow out of the marginal basin, usually through a sill or a constriction, and descends the continental slope as a gravity density current. The level at which the dense water, originated in the marginal sea, equilibrates depends on its initial density and the amount of mixing and entrainment that occurs between the dense water and the lighter water above it. Entrainment into the density current can set the bottom ocean density or in general the ocean stratification through a balance between upwelling of the dense water and downward diffusion of heat. The processes that regulate the entrainment are still poorly understood and, in particular, are missing from General Circulation Models making it difficult to match the observed ocean stratification with the modeled one in the vicinity of marginal seas. Parameterizations of entrainment have been developed in the past, and the one still widely used dates more than 40 years ago (Ellison and Turner, 1959). In the present study, we compare different entrainment parameterizations, including a new one, and their effect on the dense current and basin stratification.

Mixing across an interface between two fluids is in general characterized by a density flux in two directions, meaning that entrainment as well as detrainment takes place. In the case of a turbulent dense plume flowing beneath a nearly stagnant ambient fluid, entrainment dominates over detrainment with the turbulent dense fluid 'eating' the lighter ambient fluid (Baines, 2002). The dense plume water then enters into the environment only by interleaving at the bottom of the ocean (or at its level of neutral density). This one-way 'mixing' is being used in most of today's plume- and numerical ocean models, along with an assumption of well-

mixed lower dense layer in which density, velocity, etc., are constant in the vertical (see e.g. Price and Baringer, 1994).

Oceanic observations (e.g. Fer et al., 2004; Girton and Sanford, 2003, Arneborg et al, 2004; Arneborg et al, 2006) and laboratory studies (e.g. Ellison and Turner, 1959; Cenedese et al., 2004) of entrainment in density currents show a strong dependence on the Froude number, i.e. the ratio of the current velocity to the phase speed of long internal gravity waves. For Froude numbers larger than one, i.e. supercritical flow, the gravity currents become unstable and have a tendency to develop shear billows associated with strong entrainment (Ellison and Turner, 1959). More recently it has also been discovered that a type of breaking roll-waves may induce mixing in a dense current on a sloping bottom (Cenedese et al., 2004). Besides these (experimental) observations, similar waves have also been observed in numerical simulations (Ezer, 2005) and in large lakes (see e.g. Fer et al., 2002; Fer et al., 2001), where they were also associated with elevated mixing levels. Our knowledge of mechanisms that cause entrainment in subcritical flows is, however, limited. It is evident that oceanic density currents become diluted to a certain extent even though these are subcritical (see e.g. Duncan et al., 2003; Girton and Sanford, 2003; Fer et al., 2004), but little is known of the mechanisms of such subcritical entrainment. A laboratory experiment with comparatively small Froude numbers ($0.1 < Fr < 4$) recently showed that entrainment does also take place in a subcritical density current (even though the entrainment rate is small in comparison to a supercritical flow) (Cenedese et al., 2004).

In this study, we examine how different entrainment mechanisms influence the plume water density, and what consequences this has on the ocean stratification. A dense turbulent plume that entrains water from the surrounding fluid can build a stable stratification in a closed

container as was shown by Baines and Turner (1969). The stratification is built as the plume deposits a mixture of source- and basin water on the bottom of the tank. Layers of old plume water are pushed up toward the surface but get entrained and re-circulated during the ascent. The plume water that reaches the bottom consequently contains an increasing fraction of dense source water and the basin density will increase with depth as well as in time. The turbulent plume studied by Baines and Turner produced a basin density that (after the initial adjustment) increased linearly with time but had a constant stratification shape. The stratification and time dependence naturally depend on how much and where entrainment occurs.

The aim of the present investigation is to see how different entrainment mechanisms affect the basin stratification, in the initial transient regime for which diffusion is negligible and also for the stationary diffusive solution that is approached asymptotically in time. First, two highly simplified entrainment functions (that permit analytical solutions to the basin density equation) are studied. One with constant entrainment and one with all entrainment localized at a single depth level where the topography steepness abruptly increases. Second, two entrainment functions having a Froude number dependence are investigated. The main difference between the two functions is that one is cut off at the critical Froude number, i.e. has no entrainment at all for subcritical flow. The other function continuously decreases to zero as the Froude number approaches zero, and thus, has a small but non-zero entrainment for subcritical flow.

It is shown that the plume density is rather sensitive to the presence of this small subcritical mixing. One of the reasons is that in regions of small bottom slope, where subcritical flow may be expected, the plume has to travel a large horizontal distance in order to descend to deeper water. Consequently, the total entrainment over a level topography may not

be negligible, even though the entrainment ratio is several orders of magnitude smaller than that for supercritical flow (see also Hughes and Griffiths, 2005; and Speer and Tziperman, 1990).

As the plume water interleaves at the bottom of the basin (or at the level of neutral buoyancy) it affects the basin density. The basin stratification in the transient 'filling box' regime is highly sensitive not only to the total amount of entrainment but also to how this is distributed in the vertical, i.e. to whether it is localized to layers of steep topography or evenly spread in the whole water column. However, the stationary basin stratification that is approached asymptotically with time is not sensitive to the vertical distribution, even though the vertical variation of the plume density is. The basin stratification depends most strongly on the source plume density, the topography [i.e. the depth at which the region of maximum bottom slope is situated and how steep it is] and the surface buoyancy flux.

2. Bulk parameterizations for entrainment

As discussed above, density currents can entrain fluid from the layers above and hence increase their volume considerably. The water entrained has usually a different temperature and salinity and these properties, together with the amount of entrainment that is occurring, are of fundamental importance in determining the water properties of the dense current and ultimately the fate of such water [Price and Baringer (1994)]. The numerical global ocean circulation models that are used today resolve density currents rather poorly, and in particular, poorly calculate the mixing and entrainment that these induce. In order to represent mixing across the dense interface, it is consequently necessary to parameterize entrainment.

A successful parameterization used in the past, and still widely used to the present days, is one that assumes that the entrainment occurs in a localized region and that it depends upon the Froude number of the dense current. The entrainment velocity

$w_E = EU,$ (2.1)

is considered to be a function of the local mean velocity of the flow, U, however the function representing the entrainment coefficient E is not longer a constant. Based upon experiments by Ellison and Turner (1959) and subsequent analysis (Turner, 1986), the function E can be represented to good accuracy by

$$E = \begin{cases} \dfrac{0.08Fr^2 - 0.1}{Fr^2 + 5} & \text{for } \mathrm{Fr}^2 > 1.25 \\ 0 & \text{for } \mathrm{Fr}^2 < 1.25 \end{cases}, \quad (2.2)$$

where the Froude number is defined as

$$Fr^2 = \frac{U^2}{g'h} = \frac{g'\alpha^2}{f^2 h}, \quad (2.3)$$

where U is the plume velocity, g' is the reduced gravity, h is the plume thickness, α is the slope of the bottom topography, and f is the Coriolis parameter. Oceanic large-scale density currents are generally in geostrophic balance and flow basically parallel to the depth contours with the geostrophic velocity

$U = g'\alpha/f,$ (2.4)

(see e.g. Price and Baringer, 1994; MacCready, 1994; and Smith 1975). Bottom friction removes energy from the current and makes it descend at a small angle to the horizontal (see e.g. MacCready, 1994; Price and Baringer, 1994; Wåhlin and Walin, 2001).

The novelty of this parameterization is that it couples the entrainment to the dynamics of the dense current. It is worth noticing the strong dependence of the Froude number on the

slope α and the dependence on the density difference (i.e. g'). Since entrainment becomes non-zero only when Fr exceeds 1.25, in practice, entrainment will occur when the topography is steep or when the density difference between the dense current and the above layers is large. These conditions will increase the velocity of the dense current and consequently the Froude number of the current leading to a localized mixing when Fr>1.25. Given the variable steepness of the bottom slopes in the ocean, we should expect entrainment not only to be localized near the steep slopes, but also highly intermittent as shown by Price and Baringer (1994) and Price et al., (1993).

Fig. 1 shows the Ellison and Turner (1959) experiments together with expression (2.2) (black line). Furthermore, Fig. 1 shows observational data from four different overflows, non-rotating laboratory experiments from Alavian and Asce (1986) and recent laboratory experiments for a rotating dense current flowing down a slope (Cenedese et al., 2004). The dependence of the entrainment function E on the Froude number is clear. However, functions different from expression (2.2) could be used, if considering only the observational data a function $E = 10^{-3} Fr^{8}$ is more appropriate (Price personal communication). The recent laboratory experiments of Cenedese et al., (2004) consider a dense current flowing down a slope for relative small Froude numbers when compared to Ellison and Turner (1959) experiments. The dense current was not a turbulent plume but instead consisted of a series of breaking "roll waves." Cenedese et al., (2004) observed that the mixing between the dense current and the overlying fluid was enhanced when passing from the "laminar" to the "wave" regime, that is, with increasing Froude number. Mixing was believed to be caused by breaking waves. The entrainment function that these experiments suggest is

$$E = 4 \cdot 10^{-4} Fr^{3.5}, \qquad (2.5)$$

and, for a fixed Froude number, it presents a lower entrainment velocity when compared to the observational data (Fig. 1). Compared to the Ellison and Turner (1959) parameterization, it presents a higher (lower) entrainment velocity for subcritical (supercritical) flows.

3. A toy model

Fig. 2 shows a sketch of an ocean basin that is connected to a marginal sea where dense water is formed. Buoyancy is added to the water in the large basin and removed in the marginal sea. It is assumed that the buoyancy flux B [kg/m/s^3] over the large basin is constant, while the water in the marginal sea adjusts to a dense equilibrium value ρ_0. Furthermore, the density in the basin interior (i.e. far away from the dense plume) is assumed independent of x and y. Then the density equation in the basin is given by

$$\frac{\partial \rho}{\partial t} + w\frac{\partial \rho}{\partial z} = \kappa \frac{\partial^2 \rho}{\partial z^2}, \qquad (3.1)$$

$$\kappa \frac{\partial \rho}{\partial z} = -F_B \qquad \text{at} \qquad z = 0, \qquad (3.2)$$

$$\rho = \rho_B \qquad \text{at} \qquad z = -H, \qquad (3.3)$$

where ρ is the density, w is the vertical velocity, κ is the (constant) diffusion coefficient, $F_B = B/g$ [kg/s/m^2] is a constant and ρ_B is the density in the bottom of the basin where z = -H (where H is the maximum depth, which is constant and given in Table 1). Eq. (3.1) describes how dense bottom water is advected upwards while buoyancy from above is diffused downwards. The relative importance of the terms depends on the flushing time τ_F of the basin (where $\tau_F \sim H/w$). When τ_F is small compared to the diffusive time-scale τ_D (where $\tau_D \sim H^2/\kappa$), then the two terms on the left will dominate the equation. However, when τ_F is large compared

to τ_D, then the diffusion term on the right becomes important and a stationary solution is approached.

It is now assumed that bottom water is fed into the basin by a dense plume or a narrow sinking region. If the plume is entraining ambient water on its way down to the ocean bottom, the plume density will decrease as it becomes diluted with the ambient lighter water. However, provided the basin water initially is homogeneous and lighter than the dense source, the plume will continue to be denser than the basin at all subsequent times (e.g. Baines and Turner, 1969; Stigebrandt 1987). Consequently, the plume will always land on the bottom, and there can be no interleaving of plume water at shallower depths (unless there is more than one source). However, by postulating a detrainment ratio, portions of the dense water can be sliced off and mixed with the environment even though the plume is denser than its surroundings (see e.g. Stanev et al., 2004; Speer and Tziperman, 1990).

Mass conservation in the plume gives

$$\frac{\partial}{\partial z}(\rho_P Q_P) = \rho \frac{\partial Q_P}{\partial z}, \tag{3.4}$$

$$\rho_P(0) = \rho_0, \tag{3.5}$$

where ρ_P is the plume density, Q_P is the downward plume transport, and ρ_0 is the marginal sea (source) density. It is assumed that the plume only occupies a small portion of the basin area. The vertical velocity in the basin is then given by

$$w(z,t) = \frac{Q_P(z,t)}{A}, \tag{3.6}$$

where A is the basin area (assumed constant, see Table 1) and $Q_P(z,t)$ is the total downward plume transport at level z. In order to solve (3.1)−(3.6) we only need information about Q_P, and it is not necessary to resolve the plume path, geometry or velocity. As will be discussed in

Section 4.3, the plume properties are, however, needed to arrive at a more realistic parameterization of Q_P.

For simplicity it is assumed that the plume density and the plume downhill velocity are constant in the horizontal directions. The obtained results can be applied to a more general plume by defining $\rho_P(z,t)$ as the horizontally averaged plume density, and $Q_P(z,t)$ the horizontally integrated vertical velocity in the plume. Baines and Turner (1969) used the horizontal average based on a Gaussian profile of plume velocity and density. Other assumptions about plume properties shape will satisfy equation (3.4) but naturally a different definition of $\rho_P(z,t)$ and $Q_P(z,t)$ will be necessary (see e.g. Stanev et al., 2004).

Following the results by Baines and Turner (1969) the lower boundary condition (3.3) is

$$\rho_B = \rho_P(-H)\,. \tag{3.7}$$

Given a function $Q_P(z,t)$ we can solve the equation system (3.1) - (3.6) numerically, and under certain simplifications analytical solutions may also be found.

Consider first the solution to (3.1) with no diffusivity. By ignoring the diffusion term in (3.1), the degree of the equation is reduced and it is only possible to satisfy one of the boundary conditions. It is the upper condition (at z = 0) that must be dropped, since the basin water is advected from below. Without diffusion from above, it is not possible to control the surface density. Using (3.1)−(3.7) the system to be solved is

$$\frac{\partial \rho}{\partial t} + \frac{Q_P(z,t)}{A}\frac{\partial \rho}{\partial z} = 0\,, \tag{3.8}$$

$$\rho(z, t=0) = \rho_I\,, \tag{3.9}$$

$$\rho(-H) = \rho_P(-H), \tag{3.10}$$

$$\frac{\partial}{\partial z}(\rho_P Q_P) = \rho \frac{\partial Q_P}{\partial z}, \tag{3.11}$$

$$\rho_P(0) = \rho_0, \tag{3.12}$$

where $\rho_I < \rho_0$ is the constant initial density in the basin. If the function Q_P is independent of time, the solution to (3.8) can be written in terms of a similarity variable η,

$$\rho(z,t) = F(\eta), \tag{3.13}$$

$$\eta(z,t) = \int_{-H}^{z} \frac{A d\xi}{Q_P(\xi)} - t .$$

The function $F(\eta)$ is determined from the initial condition (3.9) (for $0 < \eta < \int_{-H}^{0} \frac{A}{Q_P(\xi)} d\xi$) and from the boundary condition (3.10) at $z = -H$ (for $\eta < 0$). Consequently the (time-dependent) plume density must be calculated in order to determine $F(\eta)$. In an initially homogeneous basin, for which ρ_I is constant, the initial plume density can be found by integration of (3.11) (using (3.12)),

$$\rho_P(z,0) = \rho_I + \frac{Q_0}{Q_P(z)}(\rho_0 - \rho_I), \tag{3.14}$$

where Q_0 is the source transport, i.e. $Q_P(0)$. At subsequent times the plume equation (3.11) has to be solved numerically at each time-step (however, for certain $Q_P(z)$ analytical solutions may be found).

According to (3.8) and (3.13), the local time-scale depends on the velocity distribution deeper down in the basin. The most rapid adjustment is expected close to the bottom where Q_P is largest. If w increases monotonically with depth, then the maximum time-scale (i.e. slowest adjustment) is at the surface and approximately given by

$$\tau_F = \frac{H}{w_0}, \tag{3.15}$$

where $w_0 = \frac{Q_P(0)}{A}$ is the vertical velocity at z = 0. The adjustment time-scale in the surface is expected to decrease if Q_P increases significantly close to the surface.

Next, consider the steady diffusive solution to (3.1), given by (3.4) and the stationary equivalent of (3.1)−(3.3), i.e.

$$\frac{Q_P(z)}{A}\frac{\partial \rho}{\partial z} = \kappa \frac{\partial^2 \rho}{\partial z^2}, \tag{3.16}$$

$$\kappa \frac{\partial \rho}{\partial z} = -F_B \qquad \text{at} \qquad z = 0, \tag{3.17}$$

$$\rho = \rho_P(-H) \qquad \text{at} \qquad z = -H. \tag{3.18}$$

The plume density is found by vertical integration of (3.4) from *z* to *0* [using integration by parts and replacing $\frac{\partial \rho}{\partial z}$ with $\frac{\kappa A}{Q_P(z)}\frac{\partial^2 \rho}{\partial z^2}$ according to (3.16)],

$$\rho_P(z) = \rho(z) + \frac{Q_0}{Q_P(z)}\left[\rho_0 - \rho(0) + D_0\left(\frac{\partial \rho}{\partial z}\bigg|_{z=0} - \frac{\partial \rho}{\partial z}\right)\right], \tag{3.19}$$

$$D_0 = \frac{\kappa}{w_0},$$

where D_0 is the diffusive depth based on w_0, i.e. the vertical velocity at $z = 0$. By evaluating (3.19) at $z = -H$, we see immediately that provided there is no heat flux through the bottom (i.e. $\frac{\partial \rho}{\partial z} = 0$ at $z = -H$), the surface density $\rho(0)$ is given by

$$\rho(0) = \rho_0 + D_0 \frac{\partial \rho}{\partial z}\bigg|_{z=0},$$

or [using (3.2)]

$$\rho(0) = \rho_0 - \frac{F_B}{w_0}. \qquad (3.20)$$

Consequently, the surface density in the basin is given by (3.20), regardless of any entrainment or detrainment that takes place deeper down. That the value of the density as well as its derivative is fixed at z = 0 poses a rather strict condition on $\rho(z)$ close to the surface. A Taylor expansion of $\rho(z)$ around $z = 0$ shows that all solutions converge to a single curve for $z << D_0$.

If there is no entrainment, then $Q_P(z) = Q_0$ and the solution to (3.16) is the exponential solution

$$\rho_M(z) = \rho_0 - \frac{F_B}{w_0} e^{\frac{z}{D_0}}, \qquad (3.21)$$

similar to that found by Munk (1966). All solutions, regardless of entrainment, hence converge to the no-entrainment solution (3.21) in the surface layer. This result can also be seen in the study by Stanev et al., (2004), in which entrainment- and detrainment ratios were varied but the obtained solutions all converged in the surface layer.

4. Results for different entrainment parameterizations

Following the results in Section 2, we anticipate that $Q_P(z,t)$ depends on the bottom slope, and that it will increase most rapidly in regions of steep topography. On the other hand, we are not certain of how strong the dependence is. For vertical plumes, the vertical rate of increase of plume transport is approximately constant (Baines and Turner, 1969). It was shown in Wells and Wettlaufer (2005) that this also holds for (non-rotating) density currents on an inclined plane and by Hughes and Griffiths (2005) that all plumes, including rotationally

influenced, can be expected to have a linear increase of plume transport in *z* provided the bottom slope is constant (see also Speer and Tziperman, 1990).

We will proceed to test three different scenarios; (i) linearly increasing $Q_P(z)$, i.e. no dependence on the variable topography, (ii) an abrupt increase of $Q_P(z)$ at a specific level z_0, i.e. very strong dependence on the variable topography, and (iii) two Froude-number dependent parameterizations according to Section 2. The two simplified functions in cases (i) and (ii) are time-independent and permits analytical solutions to (3.8) and (3.16). It is shown that the choice of function has great consequence for the basin stratification in the initial transient regime. However, the stationary diffusive solution that is approached asymptotically with time is much less sensitive to the vertical distribution of entrainment. These results also hold for more complex entrainment functions, as confirmed by the numerical solutions based on the two Froude-number parameterizations (2.2) and (2.5). The two parameterizations give rise to different plume densities, which affect the basin densities in the transient stage. Considering the difference between the obtained plume densities the stationary solutions are remarkably similar (as was also noted in Stanev et al., 2004).

4.1. Results for constant entrainment

Assume that the downward plume transport is given as a pre-defined linear function of z by

$$Q_P(z) = Q_0(1 - \gamma \frac{z}{D_0}), \tag{4.1}$$

where Q_0 is the downward plume transport at $z = 0$ and γ is a constant describing the entrainment rate. The similarity variable η [cf. expression (3.13)] is then given by

$$\eta = -\frac{\gamma}{w_0 D_0} \ln\left[\frac{1-\gamma\frac{z}{D_0}}{1+\gamma\frac{H}{D_0}}\right] - t\,. \qquad (4.2)$$

The plume density equation (3.11) has to be solved numerically for the case of constant entrainment. The solution has been plotted together with (3.13) (using (4.2)) in Fig. 3 for different γ (other parameter values as specified in Table 1). In similarity with the 'filling box' solution found by Baines and Turner (1969), we note the existence of the sharp 'first front' and how it moves upward. This front is produced by the initial density jump at $z = -H$ between plume and basin. If the basin initially has a density that increases continuously with z and becomes equal to the plume density at $z = -H$, there is no density jump and no front. Below the front, as a consequence of the entrainment and recirculation of basin water in the plume, the water is stably stratified. After the passage of the front the density difference between basin and plume decreases with time and depth. The solution asymptotically approaches the steady state $\rho = \rho_0$, as the basin fills with water containing a successively larger ratio of source water (density ρ_0). This is in contrast to the solution studied by e.g. Baines and Turner (1969), in which the source density was increased to keep a constant buoyancy flux. The most notable effect of increasing the entrainment ratio γ is that the initial density step at the 'first front' becomes smaller. This is because the plume for large γ becomes more diluted by basin water and its density more similar to the basin density [cf. eq. (3.19)]. The time to fill the basin with source water is comparable to the flushing time τ_F [cf. eq. (3.15)], regardless of the value of γ.

Next, consider the stationary diffusive equation (3.16)−(3.18). The solution (originally found by Wells and Wettlaufer (2005), but here modified to the new boundary conditions) is given by

$$\rho(z) = \rho_B - \frac{F_B}{w_0} e^{\frac{1}{2\gamma}} \sqrt{\frac{\pi}{2\gamma}} \left(erf\left[\sqrt{\frac{\gamma}{2}} \left(\frac{z}{D_0} - \frac{1}{\gamma} \right) \right] - erf\left[\sqrt{\frac{\gamma}{2}} \left(\frac{-H}{D_0} - \frac{1}{\gamma} \right) \right] \right), \tag{4.3}$$

where *erf(x)* is the error function defined as

$$erf(x) \equiv \frac{2}{\sqrt{\pi}} \int_0^x e^{-t^2} dt .$$

It remains to determine the deep basin density ρ_B. For this purpose we need to confirm that there is no buoyancy flux through the bottom. Derivation of (4.3) with respect to z gives

$$\frac{\partial \rho}{\partial z} = -\frac{F_B}{\kappa} e^{\frac{z}{D_0}\left(1 - \frac{\gamma}{2}\frac{z}{D_0}\right)}, \tag{4.4}$$

and we see that the criterion is satisfied provided $\frac{H}{D_0} >> 1$. It is now assumed that

$$\frac{H}{D_0} >> 1. \tag{4.5}$$

The surface density is then given by (3.20), and by evaluating (4.3) at $z = 0$ (combining with (3.20)), ρ_B is found as

$$\rho_B = \rho_0 - \frac{F_B}{w_0} \theta_L(\gamma), \tag{4.6}$$

$$\theta_L(\gamma) = \left(1 - e^{\frac{1}{2\gamma}} \sqrt{\frac{\pi}{2\gamma}} \left(1 - erf \sqrt{\frac{1}{2\gamma}}\right)\right).$$

The function $\theta_L(\gamma)$ increases monotonically from zero (for $\gamma = 0$) to one (for $\gamma >> 1$). Hence, the deep water density is equal to ρ_0 (the dense source density) for $\gamma = 0$ and decreases and approaches the basin surface density $\rho_0 - \frac{F_B}{w_0}$ asymptotically as $\gamma \to \infty$. It can be noted that the deep water, as well as the surface, density is independent of κ (as long as the criterion (4.5)

is satisfied), even though the stratification closer to the surface depends strongly on it [cf. expression (4.3)].

The plume density is found by combining (3.19), (4.3) and (4.4),

$$\rho_P(z) = \rho_0 - \frac{F_B}{w_0}(1 + e^{\frac{1}{2\gamma}}\sqrt{\frac{\pi}{2\gamma}}(erf\sqrt{\frac{1}{2\gamma}} + erf\left[\sqrt{\frac{\gamma}{2}}(\frac{z}{D_0} - \frac{1}{\gamma})\right]) - \frac{e^{\frac{z}{D_0}(1-\frac{\gamma}{2}\frac{z}{D_0})}}{(1-\gamma\frac{z}{D_0})}). \qquad (4.7)$$

The solutions (4.7) and (4.3) have been plotted in Fig. 4 for different values of γ and κ. As expected, solutions with different values of κ but the same γ approaches the same density as $z \to -H$. This value decreases with increasing γ. Furthermore, the surface density remains constant [cf. equation (3.20)] but the surface stratification is weaker for the larger κ. It can also be noted that the different solutions for the basin density (dashed lines in Fig. 4) corresponding to different γ (but the same κ) converge close to the surface. The curves can be compared to the non-entraining exponential solutions (3.21) obtained for $\gamma = 0$, which are also shown (thick gray lines in Fig. 4). All curves converge to these solutions in the surface, but approach the density ρ_B rather than ρ_0 in the deep basin.

Below the diffusive layer the basin- as well as plume densities are constant and equal. The plume still entrains ambient fluid but it is entraining water of the same density which naturally has no effect on either plume or basin. In fact, it becomes pointless to distinguish between plume and basin water below the diffusive layer, where their densities are equal. An important result may be postulated: *In a steady-state, the plume can only be denser than the environment in the upper layer, where the basin water gains buoyancy by diffusion from the surface.* Deeper down the plume and the environment have the same density and cannot be distinguished from each other. Hence, in a stationary system, dense plumes are only expected

to be found in a stratified environment, which is maintained by diffusion from above. By inserting (3.20) in (3.19) [if $\frac{\partial \rho}{\partial z} = 0$ then (3.19) reduces to $\rho_P = \rho$, i.e. plume- and basin densities are equal], it can be shown that this result is obtained regardless of the structure of the function Q_P.

4.2. Results for localized entrainment

Assume now that all mixing takes place at a specific depth level, $z = z_0$, where the topography abruptly steepens. The downward plume transport is then given as a step function in z, i.e.

$$Q_P(z) = \begin{cases} Q_0 & z \geq z_0 \\ Q_0(1+\gamma) & z < z_0 \end{cases}, \tag{4.8}$$

where γ is a constant. Using (3.13), the similarity variable η becomes

$$\eta = \begin{cases} \dfrac{(z_0 + H)}{w_0(1+\gamma)} + \dfrac{z - z_0}{w_0} + \mathrm{t} & z > z_0 \\ \dfrac{(z+H)}{w_0(1+\gamma)} + t & z \leq z_0 \end{cases}. \tag{4.9}$$

The plume density is given by

$$\rho_P = \begin{cases} \rho_0 & z > z_0 \\ \dfrac{\rho_0 + \gamma\rho(z_0)}{1+\gamma} & z \leq z_0 \end{cases}, \tag{4.10}$$

which has been plotted together with (3.13) (using (4.9)) in Fig. 5 for different γ (other parameter values as specified in Table 1). In similarity with the constant entrainment case (Fig. 3), we note the first front that progresses upward in time. However, the fluid below the first front is not stratified since there is no recirculation of plume water below the front. Instead

the plume density remains constant until the first front reaches the entraining level z_0. Then the mixture of plume-and basin water gets entrained into the plume which becomes denser and produces a second front at the bottom. The process continues with successively smaller density jumps and successively denser basin water. The stationary solution $\rho = \rho_0$ is also here approached asymptotically with time.

Fig. 6 shows the same calculations but with z_0 situated at a deeper level. The stair-like structure developing from the fronts is similar. However, as can be seen, the thickness of the stair-steps has decreased, due to the smaller distance traveled by each front before the succeeding front develops. The overall time-scale before the basin fills with dense source water is τ_F given by (3.15) for both cases.

Next, the stationary diffusive basin equation is given by (3.16) and (4.8) i.e.

$$w_0 \frac{\partial \rho}{\partial z} = \kappa \frac{\partial^2 \rho}{\partial z^2} \qquad \text{for } z > z_0, \tag{4.11}$$

$$w_0 (1+\gamma) \frac{\partial \rho}{\partial z} = \kappa \frac{\partial^2 \rho}{\partial z^2} \qquad \text{for } z < z_0,$$

$$\kappa \frac{\partial \rho}{\partial z} = -F_B \qquad \text{at} \quad z = 0, \tag{4.12}$$

$$\rho = \rho_P(-H) \qquad \text{at} \quad z = -H. \tag{4.13}$$

The solution can be found by matching the solutions above and below the entrainment level z_0,

$$\rho(z) = C_1 e^{\frac{z}{D_0}} + C_2 \qquad \text{for } z > z_0, \tag{4.14}$$

$\rho(z) = C_3 e^{\frac{z(1+\gamma)}{D_0}} + C_4$ for z < z_0 .

By using the matching conditions ($\rho(z_0)$ and $\left.\frac{\partial \rho}{\partial z}\right|_{z=z_0}$ continuous), it is seen that the coefficients

are related according to

$$C_3 = \frac{C_1}{1+\gamma} e^{-\gamma \frac{z_0}{D_0}}, \tag{4.15}$$

$$C_4 = C_1 \frac{\gamma}{1+\gamma} e^{\frac{z_0}{D_0}} + C_2 . \tag{4.16}$$

From the upper boundary condition we have that

$$C_1 = -\frac{F_B}{w_0} . \tag{4.17}$$

Assuming that (4.5) holds, the surface density is given by (3.20). Evaluating (4.14) at z = 0 (using (4.17)) accordingly gives

$$C_2 = \rho_0 , \tag{4.18}$$

which (using (4.14), (4.16) and (4.5)) gives the deep basin density ρ_B. The result is

$$\rho_B = \rho_0 - \frac{F_B}{w_0} e^{\frac{z_0}{D_0}} \theta_S(\gamma) , \tag{4.19}$$

$$\theta_S(\gamma) = \frac{\gamma}{1+\gamma} .$$

Consequently, in similarity with the case of constant entrainment, the deep water density decreases asymptotically from ρ_0 (for $\gamma = 0$) to $\rho_0 - \frac{F_B}{w_0}$ as $\gamma \to \infty$. The entrainment has to take place in the diffusive surface layer in order to be effective (as can be seen by the

exponential decrease of the coefficient $e^{\frac{z_0}{D_0}}$ with z0 in (4.19)). Furthermore, for a given $\frac{z_0}{D_0}$, the surface as well as the deep basin density is independent of κ.

The plume density is given by (3.19) or

$$\rho_P = \rho_0 \qquad \text{for } z > z0, \qquad (4.20)$$

$$\rho_P = \rho_0 - \frac{F_B}{w_0}\theta_S(\gamma) \qquad \text{for } z < z0,$$

where $\theta_S(\gamma)$ is given by (4.19).

The solutions (4.20) and (4.14) [using (4.15)−(4.18)] have been plotted in Fig. 7 for different values of γ and κ (keeping $\frac{z_0}{D_0}$ constant and equal to -1). As expected the solutions with different κ but same γ approach the same value ρ_B as $z \to -H$. As γ is increased, ρ_B decreases. The surface density remains constant [cf. equation (3.20)] but the surface stratification becomes weaker as κ is increased.

4.3. Results for a plume parameterization of entrainment

The solutions obtained in sections (4.1) and (4.2) illustrate what to expect in the two cases of localized and constant entrainment. However, these two idealized cases are not very realistic for the ocean where there is, as discussed in Section 2, strongest entrainment close to the dense source and over steep topography (where the current speeds up). The two-dimensional evolution of plume path, geometry etc. can be obtained by use of so-called stream-tube models (see e.g. Smith, 1975; Killworth, 1977, Price and Baringer, 1994; Borenäs and Wåhlin, 2000), in which the outflow properties are assumed to vary only along the outflow

path. As a result of this assumption the plume geometry is not fully resolved, and additional assumptions have to be made regarding the plume width and/or thickness (e.g. by specifying the evolution of the outflow width, as was done in Price and Baringer (1994), or specifying the aspect ratio, as was done in Killworth, 1977). When the plume entrains the surrounding water its volume flux increases, which entails an increased cross-sectional area and/or plume velocity and a decrease of the density difference between plume and ambient water. The models all give realistic results in the outflow regions, but naturally fail when the plume water becomes too diluted by the basin water since the dense plumes do not interleave into the environment. Evidence from laboratory experiments (Baines, 2001; Baines, 2002; Baines, 2005; Pierce and Rhines, 1996) as well as observations (Stanev et al, 2004; Ambar and Howe, 1979) indicate that the plume water does interleave and detrain when the density difference becomes sufficiently small.

In the present study the plume is coupled to a one-dimensional basin. Hence, we only need information about the total entrainment that takes place at a certain depth level, i.e. $Q_P(z)$. By integrating the entrainment velocity w_E along a closed depth contour, $Q_P(z)$ is given by

$$Q_P(z) = Q_0 + \int_z^0 \oint_{C(x,y)} \frac{w_E}{\sin\alpha} dl d\xi , \qquad (4.21)$$

where $C(x,y)$ is a closed depth contour, w_E is the entrainment velocity, and α is the bottom slope (derivation can be found e.g. in Hughes and Griffiths, 2005; and Speer and Tziperman, 1990).

Assume now that the plume velocity as well as its density and entrainment velocity only varies with z. Then (4.21) is given by

$$Q_P(z) = Q_0 + \int_z^0 L(\xi) \frac{w_E(\xi)}{\sin \alpha(\xi)} d\xi \,, \tag{4.22}$$

where *L(z)* is the arc-length that the plume occupies or the plume width along a constant depth contour. It may be noted that equation (4.22) does not contain or utilize any information about the plume besides the arc-length *L* and the entrainment velocity w_E. Specifically, there is no information about *how* the entrained water is accommodated in the plume.

Observations (e.g. MacCready, 1994; Smith, 1975; Price and Baringer, 1994) show that the dense overflows are basically in geostrophic balance, i.e. the along-slope velocity component is given by (2.4) and the down-slope velocity component is small in comparison. Furthermore, observations (e.g. Duncan et al, 2003, Girton and Sanford, 2003, Price and Baringer, 1994; Smith, 1975) of the outflow thickness show that although this varies quantitatively in time as well as in space it does not vary qualitatively in the outflow region. Hence, in order to simplify the description, it is assumed that the plume velocity $V_P(z)$ is given by

$$V_P = \sqrt{U^2 + w_P^2} \tag{4.23}$$

$$U >> w_P \,, \tag{4.24}$$

where *U* is given by (2.4) and w_P is the downward velocity component. It is furthermore assumed that *h* is constant. The Froude number is then given by (2.3). In order to obtain the entrainment velocity w_E from (2.1) an assumption has to be made regarding the entrainment function *E(Fr)*. As argued in Section 2, the experimental and observational data can be fitted to different curves and we will study the two functions (2.2) and (2.5). The main difference between them is that (2.2) has no entrainment at all for sub-critical flows, while (2.5) decreases

asymptotically to zero for small *Fr*. As will be shown, the seemingly small difference in *E(Fr)* has consequences for the basin density.

As mentioned above, (4.22) does not contain any information about how the entrained volume flux is accommodated in the plume. Under the assumptions made so far, i.e. (4.23) - (4.24), (2.4), constant h, and only z-dependence of the plume properties, an increased volume flux in the plume is accommodated by an increase of w_P (cf. eq. (4.23)) and/or an increase of L. We now take L to be constant, which is a rather rough simplification. However, the obtained solutions are not particularly sensitive to the value of L, as was seen by comparing the present results to those obtained with a 5 times larger L. This reduces the deep basin density but only by less than 10 % of the surface values, and for most cases less than 3 % (not shown here). The insensitivity of the solutions to the value of L indicates that the variations of *E(Fr)* as the velocity increases (over steep topography) or decreases (as a result of entrainment or by leaving the steep region) are sufficiently large (in the present examples) to be the dominating important effect. However, if L is constant it means that the increased volume flux due to entrainment is accommodated by an increased w_P, and the assumption (4.24) eventually becomes violated. This happens when g' (and thereby U) becomes sufficiently small and/or $Q_P(z)$ sufficiently large. In the subsequent calculations it was assumed that (4.24) was valid. After performing the calculations condition (4.24) was checked and the level at which it became violated (i.e. where $U = w_P$) was identified. The density difference between plume and basin at that level gives an upper estimate of the error made by ignoring the w_P term in (4.23). This error was less than 21 % of the surface plume-basin density difference for all calculations, i.e. far below the uncertainty expected in this highly simplified model.

Provided L is constant then (4.21) can be written

$$Q_P(z) = Q_0 + L\int_z^0 \frac{w_E}{\sin\alpha} dz \,. \qquad (4.25)$$

Furthermore, it is assumed that the bottom slope α varies with z according to

$$\alpha(z) = \alpha_1 e^{-\frac{(z-z_0)^2}{d^2}} + \alpha_2 \,, \qquad (4.26)$$

where $\alpha_{MAX} = \alpha_1 + \alpha_2$ is the steepest slope (situated at level z_0), α_2 is the minimum slope and d is the thickness of the steep region.

As described here, the plume moves basically along the depth contours in geostrophic balance, descending at a small angle induced by bottom friction. This behavior is to be expected of ocean scale density currents (see e.g. Price and Baringer, 1994; MacCready, 1994; and Wåhlin and Walin, 2001). When the plume moves into a region of steep topography, it speeds up and the Froude number increases [cf. eq. (2.3)]. The entrainment coefficient, E, then increases, and the plume entrains ambient fluid which reduces the density difference and the Froude number. After passing the region where the bottom slope has its maximum value, the velocity will decrease because of the smaller slope but also because of the smaller density anomaly, and the entrainment levels are expected to be comparatively small.

Using (2.3) the density difference where the flow becomes subcritical is expected to be close to $\Delta\rho_{CR}$ given by

$$\Delta\rho_{CR} = \frac{f^2 h \rho_0}{g\alpha_{MAX}^2} Fr_{CR}^2 \,, \qquad (4.27)$$

where Fr_{CR}^2 = 1.25 is the critical Froude number according to (2.2) and α_{MAX} is the maximum bottom slope. The value of α_{MAX} will determine the total rate of entrainment for (2.2) (and hence the density of the deep water) according to (4.27).

The two functions (2.2) and (2.5) will now be tested and compared for the time-dependent as well as the stationary case. The main difference between the two is that (2.5) approaches zero asymptotically as $Fr \to 0$, while (2.2) is identically zero for subcritical Froude numbers. Fig. 8 shows the time development of the basin- and plume densities as calculated numerically from (3.8)−(3.12) (using (4.25) and (4.26)), together with the obtained function $Q_P(z,t)$. In similarity with the constant entrainment (section 4.1) and the localized entrainment (section 4.2) there is a 'first front' that moves up through the water column. Due to numerical diffusion it is however smoothed compared to the analytical cases. The difference in plume density that results from using entrainment function (2.2) or (2.5) is noticeable, in particular in the top 1000 m. The reason is that the subcritical entrainment that the plume experiences with parameterization (2.5) takes place over a large distance. Since the bottom slope is small, the plume travels a large horizontal distance in order to descend to deeper levels (as can be seen by the presence of the term $\sin(\alpha)$ in the denominator of (4.21) (Hughes and Griffiths, 2005; Speer and Tziperman, 1990). Consequently the entrainment is more localized to the steep region when parameterization (2.2) is utilized, while parameterization (2.5) is more spread in the vertical.

In the steady-state regime, it is expected (from the analytical results in the previous sections) that the surface basin density will be close to the no-entrainment solution (3.21) for both entrainment parameterizations. However, in the deep basin the value ρ_B should be approached rather than ρ_0. It is also expected that the entrainment must take place in the diffusive surface layer in order for it to have any effect on the basin stratification. Hence, ρ_B may be estimated as (using (4.27))

$$\rho_B = \rho_M + \frac{f^2 h \rho_0}{g \alpha_{MAX}^2} Fr_{CR}^2, \qquad (4.28)$$

where ρ_M is given by (3.21) evaluated at z = z_0. By increasing α_{MAX} and moving z_0, we can increase the entrainment and move the entrainment region in order to check the prediction (4.28).

Fig. 9 shows the numerical solution to eq. (3.4) and (3.16) with $Q_P(z)$ given by (4.25) and w_E by (2.1), using the Ellison and Turner parameterization (2.2) (all constants and parameter values according to Table 1 unless otherwise stated), for different values of κ, α_{MAX} and z_0. The ratio z_0/D_0 was kept constant and equal to -1, which means that ρ_M was constant even though two different κ and z_0 were used. Horizontal lines indicate the location of z_0 and show that most of the entrainment takes place above the level z_0. The total entrainment depends strongly on the bottom slope, the steepest topography (α_{MAX} = 0.16) has a 10 e-fold increase of the plume transport. Whereas, the least steep topography (α_{MAX} =0.009) has only an increase of the plume transport of about 10% (hardly detectable in Fig. 9b). Also shown as pale colored lines are the density estimates (4.28) and as gray lines the no-entrainment solution (3.21). As can be seen, the agreement is reasonable. Fig. 10 shows the same calculation but for the parameterization (2.5). The basin densities for the two steepest topographies are remarkably similar in the two cases, even though the plume densities and transports differ. However, for the most level topography, there is a marked difference between the two cases with the deep basin water being much denser for the Ellison and Turner parameterization (in fact, the deep water is for that case nearly undiluted source water). For small enough α_{MAX}, the flow does not become supercritical. Since the maximum density difference is in the surface, we have that $Fr < Fr_{CR}$ for all depths provided $\alpha_{MAX} < \alpha_{CR}$ given by

$$\alpha_{CR} = fFr_{CR}\sqrt{\frac{h\rho_0}{g\Delta\rho_0}}, \qquad (4.29)$$

$$\Delta\rho_0 = \frac{F_B}{w_0},$$

where (3.20) has been used. The difference between the blue curves that can be seen by comparing Figs. 9 and 10, indicates that sub-critical mixing may affect the basin stratification also in the stationary state. In particular, this is to be expected if the maximum topographic slope is smaller than, or comparable to, the critical bottom slope α_{CR} (0.0046 in the examples here).

Next, a new set of calculations in which z_0 was moved to below the diffusive surface layer ($z_0 = -2D_0$) was performed. It is expected from the analytical results in preceding sections that even though entrainment may take place below the diffusive layer, it will not cause any significant changes in the basin- or the plume densities. The reason is that the difference between the two densities will always be very small below the diffusive layer. The results pertaining to the Ellison and Turner parameterization are shown in Fig. 11. Even though entrainment does take place, it has little effect on the basin density; ρ_B is for all three topographies close to the dense source value. The results for the parameterization (2.5) are similar (not shown here).

5. Discussion

A one-dimensional model for a large ocean basin to which dense water is supplied via an entraining density current has been utilized to study the effect of various entrainment parameterizations on the ocean stratification. The model is similar in set-up to the ones used by e.g. Speer and Tziperman (1990), Munk and Wunsch (1998), Stanev et al, (2004), Wells and

Wettlaufer (2005), and Hughes and Griffiths (2005). The plume originates in a marginal sea where it has a constant source density (this is in contrast to previous studies where the density difference between plume and basin, or the buoyancy flux into the basin, was kept constant). Dense plume water is deposited at the bottom of the basin, from where it is advected up towards the surface where a constant buoyancy flux is applied. During the ascent the 'old' plume water gets entrained and re-circulated in the plume, giving rise to an increase in density with depth as well as with time.

In the initial adjustment phase there is a sharp front (caused by the initial density difference between the plume and the basin bottom water) that moves up through the water column. Beneath the front the basin is stably stratified and fills with water containing an increasing fraction of dense source water. After the initial adjustment, a stationary solution in which diffusion of buoyancy from above balances the advection of dense water from below is approached.

Entrainment of basin water into the plume dilutes the plume water and increases the plume transport. To compensate for the increased transport, the vertical velocity in the basin will increase with depth, while the dilution of the plume water reduces the density in the deep basin when compared to the source density. The basin density is consequently highly dependent on the plume entrainment. The main object of this study was to test different entrainment parameterizations and see how these affect the basin density in the initial transient regime as well as in the stationary diffusive solution that is approached asymptotically with time.

The important dependence is the vertical distribution of the horizontally integrated plume downward transport which is a function of the plume entrainment. We distinguish

between constant entrainment, which can be expected in the case of constantly sloping bottom in a rotating (Hughes and Griffiths, 2005) and non-rotating system (Wells and Wettlaufer, 2005; Baines and Turner, 1969), and localized entrainment, which can be expected in the case of variable bottom topography that steepens at a certain level z_0. Two idealized functions representing these two cases were used to solve the system analytically, and the solutions were studied for different entrainment ratios, γ.

The initial adjustment on time-scales shorter than the 'filling time' $\tau_F = H/w_0$ is highly sensitive to how mixing is parameterized, as has also recently been showed in a full-scale numerical model of a density current on a sloping bottom (Legg et al., 2006). The 'first front' that moves up through the water column after the plume has been released moves with step-wise constant velocity (with the larger velocity below the entrainment level) in the case of localized entrainment, but with linearly decreasing velocity in the case of constant entrainment (in similarity with the studies of e.g. Baines and Turner 1969; Wells et al., 1999; Wells and Wettlaufer, 2005). Below the front, the stratification is continuous for the constant entrainment (again in similarity with previous studies), however, for the localized entrainment a stair-case stratification develops as the homogeneous mixture of plume- and basin water reaches the entraining level which abruptly increases the plume density. If the entrainment is spread over a larger depth range, the stair-steps become less sharp and the basin density more like the continuous stratification in the constant entrainment case (not shown). In both cases, the effect of increasing the entrainment ratio is to reduce the stratification below the first front and to increase the speed of the front. However, the time-scale at which the basins become filled with pure source water is the filling time $\tau_F = H/w_0$, regardless of entrainment rate or its vertical distribution.

After the initial adjustment, diffusion becomes important and a stationary state in which diffusion of buoyancy from above balances the advection from below is approached. All the solutions, regardless of any entrainment that takes place deeper down, then converge to a single density profile in the surface layer. The surface profile is identical to the exponential no-entrainment solution (3.21) obtained for constant vertical velocity and diffusivity, but based on the deep basin density ρ_0 (i.e. the undiluted dense source value). Below the surface the solutions diverge and approach a less dense deep basin density ρ_B, the value of which decreases by the amount of entrainment that takes place in the diffusive surface layer. These results hold for localized as well as evenly distributed entrainment and are also in line with the findings of Stanev et al., (2004) and Wells and Wettlaufer (2005).

It may be noted that a clearly identifiable plume (i.e. one that is denser than the environment) can only be found at depths to which diffusion from above reaches and the basin water is stratified. Below this level the basin is filled with the plume water that is deposited at the bottom, and the two water masses have the same density regardless of source density and how much or where the plume becomes diluted. It is only the entrainment that takes place in the diffusive surface layer that influences the deep basin density; below this depth the plume entrains water of equal density which naturally has no consequence for the density of either the plume or the basin.

Below the diffusive layer the plume has momentum but cannot otherwise be distinguished from the basin water, and there is no telling from the present model if the plume interleaves at the level of neutral density or continues to the bottom. It has been assumed that there is no continuous detrainment of plume water into the basin, in which case the plume will always interleave at the bottom (see e.g. Baines and Turner, 1969). However, as was shown by Stanev

et al., (2004), CFC measurements from the Black Sea indicate that the dense plume there does not continue to the bottom but interleaves at intermediate depths. The same was also observed by Pierce and Rhines (1996) in a laboratory experiment with a dense source flow, although numerical simulations of the same flow showed a plume that always reached the bottom (Pierce and Rhines, 1996). The assumption of no detrainment is in line with the findings of Baines (2002) for turbulent plumes, but in contrast with the findings of Baines (2001) for gentle slope flows where detrainment in fact dominated over entrainment (see also Baines, 2005). However, according to the present results the question of detrainment is only important in the diffusive surface layer. Below this level, the plume and the basin are equally dense and their densities are not affected by either entrainment or detrainment (although the distribution of tracers etc. is highly sensitive to entrainment and detrainment also below this level).

How may the above results then be applied to the ocean? Laboratory studies as well as observations indicate that the entrainment coefficient E increases with the Froude number (i.e. the ratio of the plume velocity to the speed of a long internal gravity wave), and that elevated Froude numbers are found in regions of steep topography. This is consistent since the dense plume velocity is expected to be close to the geostrophic slope velocity, $g'\alpha/f$, and increases as the plume moves into a steep region (i.e. large α). Therefore, we assume the plume velocity to be geostrophic and its thickness constant, which suggests that the total entrainment rate depends strongly on the topography, with large entrainment and strong dilution of the plume taking place at and above the level of maximum bottom slope. The plume density decreased until the Froude number was subcritical [cf. expression (4.29)] at the level of maximum bottom slope.

Two different functions that parameterize the entrainment coefficient E for various Froude numbers were employed. The main difference between the two is that E is identically zero for subcritical Froude numbers in the first, while in the second E asymptotically approaches zero for small Froude numbers. Hence, there is in the second parameterization a certain amount of mixing taking place also for subcritical flows, although it is small in comparison to supercritical entrainment. The subcritical mixing affects the plume density also in regions where the bottom slope is smaller than the critical slope α_{CR} [cf. eq. (4.29)] at which the flow becomes critical. The obtained plume densities are rather different in the shallow regions, where $\alpha < \alpha_{CR}$.

The entrainment is consequently distributed vertically above the steepest region, according to which entrainment function is utilized. The results obtained with the stationary analytical solutions for the constant and localized entrainment hold for both entrainment functions. The basin density tends to the no-entrainment solution (3.21) in the surface, regardless of the topography and the entrainment rate. Deeper down a deep basin density ρ_B is approached. The topography is important for determining ρ_B in that a steep bottom slope gives large entrainment and a less dense ρ_B. It is also important at what vertical level z_0 the steepest bottom slope is situated. If z_0 is below the diffusive layer (and the bottom slope subcritical above it), then the plume will only entrain water that is equally dense which has no effect on either plume- or basin density. If the maximum bottom slope is large compared to the critical slope α_{CR}, at which the flow becomes supercritical, then the two parameterizations of E give similar basin densities. However, if the bottom slope is comparable to or smaller than α_{CR}, then the subcritical mixing becomes important enough (in comparison to the supercritical

mixing) to significantly reduce the deep basin density (as compared to the case in which entrainment was set to zero for subcritical flow).

In summary, the findings in this paper indicate that the choice of entrainment parameterization is very important for the ocean stratification in transient regimes (as has also been shown by use of less simplified models by e.g. Legg et al., 2006; Chang et al., 2005; and Liungman et al., 2001). However, at longer time-scales, different parameterizations give similar basin stratification for a given topography (this was also noted by Thorpe et al., (2004) in a sensitivity study of a long-term climate model to the overflows over the Greenland-Scotland Ridge). The basin density is expected to be close to the exponential no-entrainment profile (3.21) in the surface, but 'cut off' at the value ρ_B (4.28) that depends on the buoyancy flux, the outflow source density and transport, the maximum bottom slope and the depth at which the topography slopes most steeply. The exception to this rule of thumb is a basin with maximum bottom slope that is less than, or comparable to, the slope α_{CR} [cf. eq. (4.29)] for which the flow is always subcritical. For such a basin it is important also in the stationary-state how the entrainment coefficient is parameterized, and in particular how it is parameterized for subcritical flows. Regrettably, there are very few studies focusing on entrainment processes in subcritical currents, and the present results indicate that these may in fact be of importance also globally. An investigation is underway by the authors in which observed basin stratification and source density are compared to the results of the present model. The results may provide a recommendation regarding the entrainment functions and their ability to parameterize ocean density current mixing.

Acknowledgements

Part of this work was funded by Göteborg University and the Swedish Research Council under the contract G600-335/2001 through Prof. A. Omstedt. Support was given to CC by the National Science Foundation project number OCE-0050891. Discussions with Pål Erik Isachsen were very much appreciated. We also gratefully appreciate the careful reading of and ideas for improvements in the manuscript by Jack Whitehead, Jiayan Yang, Lars Arneborg, and two anonymous reviewers. This is Woods Hole Oceanographic Institution contribution number 11390.

References

Alavian, V., Asce, A.M., 1986. Behavior of density currents on an incline. J. Hydrol. Eng. 112, 2742.

Ambar, I. and M. R. Howe, 1979. Observations of the Mediterranean Outflow-II. The deep circulation in the vicinity of the Gulf of Cadiz. Deep Sea Research 26A, 555 - 568.

Arneborg, L., Fiekas, V., Umlauf, L. and H. Burchard, 2006. Gravity current dynamics and entrainment - A process study based on observations in the Arkona Basin. Submitted to Journal of Physical Oceanography.

Arneborg, L., C.P. Erlandsson, B. Liljebladh, and A. Stigebrandt, 2004. The rate of inflow and mixing during deep-water renewal in a sill fjord. *Limnol. Oceanogr.*, 49, 768-777.

Baines, P.G., 2001. Mixing in flows down gentle slopes into stratified environments. Journal of Fluid Mechanics 443, 237−270.

Baines, P.G., 2002. Two-dimensional plumes in stratified environments. Journal of Fluid Mechanics 471, 315−337.

Baines, P.G., 2005. Mixing regimes for the flow of dense fluid down slopes into stratified environments. Journal of Fluid Mechanics, 538, 245 - 267.

Baines, W.D., Turner, J.S., 1969. Convection from a source in a confined region. Journal of Fluid Mechanics 37, 51−80.

Borenäs K. and A. Wåhlin, 2000. Limitations of the plume model. Deep Sea Research I, 47, 1333 - 1350.

Cenedese, C., Whitehead, J.A., Ascarelli, T.A., Ohiwa, M., 2004. A dense current flowing down a sloping bottom in a rotating fluid. Journal of Physical Oceanography 34, 188−203.

Chang, Y.S., Xu, X., Özgökmen, T.M., Chassignet, E.P., Peters, H., Fischer, P.F., 2005. Comparison of gravity current mixing parameterizations and calibration using a high resolution 3D nonhydrostatic spectral element model. Ocean Modelling 10, 342−368.

Duncan, L., Bryden, H., Cunningham, S., 2003. Friction and mixing in the Faroe Bank Channel Outflow. Oceanologica Acta 26, 473−486.

Ellison, T.H., Turner, J.S., 1959. Turbulent entrainment in stratified flows. Journal of Fluid Mechanics 6, 423−448.

Ezer, T., 2005. Topographic influence on overflow dynamics: Idealized numerical simulations and the Faroe Bank Channel overflow, J. Geophys. Res., (2005JC003195), submitted.

Fer, I., Lemmin, U., Thorpe, S.A., 2001. Cascading of water down the sloping sides of a deep lake in winter. Geophysical Research Letters 28(10), 2093−2096.

Fer, I., Lemmin, U., Thorpe, S.A., 2002. Winter cascading of cold water in Lake Geneva. Journal of Geophysical Research 107(C6), 13.

Fer, I., Skogseth, R., Haugan, P., 2004. Mixing of the Storfjorden overflow (Svalbard Archipelago) inferred from density overturns. Journal of Geophysical Research 109, C01005.

Girton, J.B., Sanford, T., 2003. Descent and modification of the overflow plume in the Denmark Strait. Journal of Physical Oceanography 33, 1351−1364.

Hughes, G.O., Griffiths, R.W., 2005. A simple convective model of the global overturning circulation, including effects of entrainment into sinking regions. Ocean Modeling, in press.

Killworth, P. 1977. Mixing on the Weddell Sea continental slope.Deep Sea Research, 24, 427 - 448.

Legg, S., Hallberg, R., Girton, J., 2006. Comparison of entrainment in overflows simulated by z-coordinate, isopycnal and non-hydrostatic models. Ocean Modelling 11, 69−97.

Liungman, O., Rydberg, L., Göransson, C.G., 2001. Modeling and Observations of Deep Water Renewal and Entrainment in a Swedish Sill Fjord. Journal of Physical Oceanography 31(12), 3401−3420.

MacCready, P., 1994. Frictional decay of abyssal boundary currents. Journal of Marine Research 52, 197−217.

Morton, B.R., 1959. Forced plumes. Journal of Fluid Mechanics 5, 151−163.

Munk, W., 1966. Abyssal recipes. Deep Sea Research 13, 707−730.

Munk, W., Wunsch, C., 1998. Abyssal Recipes II: energetics of tidal and wind mixing. Deep-Sea Research 45, 1976−2000.

Pierce, D.W., Rhines, P.B., 1996. Convective building of a pycnocline: Laboratory experiment. Journal of Physical Oceanography 26(2), 176−190.

Price, J.F., Baringer, M.O., 1994. Outflows and deep water production by marginal seas. Progress in Oceanography 33, 161−200.

Price J.F., Baringer, M.O., Lueck, R.G., Johnson, G.C., Ambar, I., Parrilla, G., Cantos, A., Kennelly, M.A., Sanford, T.B., 1993. Mediterranean outflow mixing dynamics. Science 259, 1277−1282.

Price, J.F., Yang, J., 1998. Marginal sea overflows for climate simulations. Ocean Modeling and Parameterization, E. Chassignet and J. Verron, Eds., Kluwer Academic, 155170.

Smith, P.C., 1975. A streamtube model for bottom boundary currents in the ocean. Deep Sea Research 22, 853−873.

Speer, K., Tziperman, E., 1990. Convection from a source in an ocean basin. Deep-Sea Research 37, 431-446.

Stanev, E., Staneva, J., Bullister, J., Murray, J., 2004. Ventilation of the Black Sea pycnocline. Parameterization of convection, numerical simulations and validations against observed chlorofluorocarbon data. Deep Sea Research I 51, 2137−2169.

Stigebrandt, A. 1987. A model for the vertical circulation of the Baltic Sea deep water. Journal of Physical Oceanography, 17 (10), 1772 - 1785.

Thorpe, R.B., Wood, R.A., Mitchell, J.F.B., 2004. Sensitivity of the modelled thermohaline circulation to the parameterization of mixing across the Greenland–Scotland ridge. Ocean Modelling 7, 259−268.

Turner, J.S., 1986. Turbulent entrainment: The development of the entrainment assumption and its application to geophysical flows. Journal of Fluid Mechanics 170, 431−471.

Wells, M.G., Griffiths, R.W., Turner, J.S., 1999. Competition between distributed and localized buoyancy fluxes in a confined volume. Journal of Fluid Mechanics 391, 319−336.

Wells, M.G., Wettlaufer, J.S., 2005. Two-dimensional density currents in a confined basin. Geophysical and Astrophysical Fluid Dynamics 99(3), 199−218.

Wåhlin, A.K., Walin, G., 2001. Downward migration of dense bottom currents. Environmental Fluid Mechanics 1(2), 257−279.

Table 1. Standard values of constants and coefficients used in the text. Unless otherwise stated, these values were used in the calculations on which Fig. 3−11 were based.

Notation	Dimension	Description	Standard value
f	s^{-1}	Coriolis parameter	10^{-4}
h	m	Plume thickness	100
ρ_0	kg/m^3	Dense source density	1030
Fr_{CR}	-	Critical Froude number	1.25
F_B	$kg/m^2/s$	Buoyancy flux	$-6 \cdot 10^{-7}$
Q_0	m^3/s	Source plume transport	$1 \cdot 10^6$
A	m^2	Basin area	10^{13}
w_0	m/s	vertical velocity at z = 0	10^{-7}
L	m	Arc-length occupied by plume	10^5
d	m	Thickness of steep region	250
a_{MAX}	rad	Maximum bottom slope	0.009, 0.016, 0.16
a_{MIN}	rad	Minimum bottom slope	0.0016
H	m	Basin depth	5000

Figure Captions

Fig. 1. Entrainment coefficient as a function of Froude number for observational data and experiments. Shaded areas indicate experiments from Alavian and Asce (1986) and Ellison and Turner (1959). Markers indicate observational data and experiments from Cenedese et al. (2004) according to legend. Colored lines indicate different functions fitted to the data; the black line is expression (2.2) and the green line expression (2.5). Modified from Cenedese et al., (2004) and Price and Yang (1998) with additions from Price (personal communication).

Fig. 2. Sketch of the idealized basin and some of the notations used. (a) Side view. (b) Top view.

Fig. 3. Basin (solid) and plume (dashed) density as a function of depth for five succeeding times, t1 = 0.01 τ_F, t2 = 0.1 τ_F, t3 = 0.2 τ_F, t4 = 0.5 τ_F, t5 = 1.5 τ_F where $\tau_F = H/w_0$ is the flushing time (1600 yrs). Vertical distribution of entrainment was $Q_P(z) = Q_0(1-\gamma\frac{z}{D_0})$ (i.e. constant entrainment) with Q_0 = 1 Sv, D_0 = 2500 m, and γ = 0.1. **(a)** γ = 1. **(b)** γ = 8. **(c)** Panel. **(d)** shows the three $Q_P(z)$ obtained for γ = 0.1 (blue), γ = 1 (red), and γ = 8 (green).

Fig. 4. Basin (solid) and plume (dashed) density as a function of depth for the stationary diffusive solution (4.3) and (4.7). Vertical distribution of entrainment was $Q_P(z) = Q_0(1-\gamma\frac{z}{D_0})$ (i.e. constant entrainment) with Q_0 = 1 Sv, and $D_0 = \frac{\kappa}{w_0}$. **(a)** The curves show the solution for three different γ, γ = 0.1 (blue), γ = 1 (red), and γ = 8 (green) and two different k; κ = 1.25e-4 m^2/s (lower curves) and κ = 0.5e-4 m^2/s (upper curves). Also shown as thick gray lines are the non-entraining solutions (3.21). **(b)** The curves show

the six $Q_P(z)$ obtained for κ = 1.25e-4 m^2/s (dashed), κ = 0.5e-4 m^2/s (solid), γ = 0.1 (blue), γ = 1 (red), and γ = 8 (green).

Fig. 5. Basin (dashed) and plume (solid) density as a function of depth for 5 succeeding times, t1 = 0.01 τ_F, t2 = 0.1 τ_F, t3 = 0.2 τ_F, t4 = 0.5 τ_F, and t5 = 1.5 τ_F where $\tau_F = H/w_0$ is the flushing time (1600 yrs). Vertical distribution of entrainment was localized according to (4.8) with Q_0 = 1 Sv, z_0 = -1500 m and entrainment coefficient γ = 0.1. **(a)** γ = 1. **(b)** and γ = 8. **(c)** Panel. **(d)** shows the three $Q_P(z)$ obtained for γ = 0.1 (blue), γ = 1 (red), and γ = 8 (green). Note that the line types are different from Figs. 3−4.

Fig. 6. Basin (dashed) and plume (solid) density as a function of depth for 5 succeeding times, t1 = 0.01 τ_F, t2 = 0.1 τ_F, t3 = 0.2 τ_F, t4 = 0.5 τ_F, and t5 = 1.5 τ_F where $\tau_F = H/w_0$ is the flushing time (1600 yrs). Vertical distribution of entrainment was localized according to (4.8) with Q_0 = 1 Sv, z_0 = -3500 m and entrainment coefficient γ = 0.1. **(a)** γ = 1. **(b)** and γ = 8. **(c)** Panel. **(d)** shows the three $Q_P(z)$ obtained for γ = 0.1 (blue), γ = 1 (red), and γ = 8 (green). Note that the line types are different from Figs. 3−4.

Fig. 7. Basin (solid) and plume (dashed) density as a function of depth for the stationary diffusive solution (4.3) and .(4.7) **(a)** The curves show the solution for three different γ, γ = 0.1 (blue), γ = 1 (red), and γ = 8 (green) and two different κ and z_0; κ = 1.25e-4 m^2/s and z_0 = -750 m (lower curves), and κ = 0.5e-4 m^2/s and z_0 = -250 m (upper curves). Also shown as thick gray lines are the non-entraining solutions (3.21). **(b)** The curves show the three $Q_P(z)$ obtained for γ = 0.1 (blue), γ = 1 (red), and γ = 8 (green) for both z_0 = -750 m (solid) and z_0 = -250 m (dashed). The small increase in plume transport (10 %) for the blue lines is hardly visible.

Fig. 8. Result of the Froude number parameterizations for 4 succeeding times, t1 = $0.1\,\tau_F$ (green), t2 = $0.2\,\tau_F$ (yellow) t3 = $0.5\,\tau_F$ (red), and t4 = τ_F (blue) where $\tau_F = H/w_0$ is the flushing time (1600 yrs). The maximum bottom slope α_{MAX} was 0.016 and situated at level z_0 = 1250 m; all other parameter values according to Table 1. **(a)** Basin- and plume density as a function of depth for the Ellison and Turner parameterization. **(b)** Downward plume transport as a function of depth for the Ellison and Turner parameterization. **(c)** Basin- and plume density as a function of depth for the parameterization (2.5). **(d)** Downward plume transport as a function of depth for the parameterization (2.5).

Fig. 9. Basin (solid) and plume (dashed) density as a function of depth as calculated by the numerical solution to (3.16) - (3.19), with the plume transport parameterized according to (4.25) and the Ellison and Turner entrainment function (2.2), with the velocity given by (2.4) and the bottom slope (4.26). **(a)** The curves show the solution for three different α_{MAX}; α_{MAX} = 0.009 (blue), α_{MAX} = 0.016 (red), and α_{MAX} = 0.16 (green) and two different κ and z0; κ = 1.25e-4 m^2/s and z_0 = -1250 m (lower curves), and κ = 0.5e-4 m^2/s and z_0 = -500 m (upper curves). Also shown as thick gray lines are the non-entraining solutions (3.21) and $\Delta\rho_{CR}$ as calculated by (4.28) for α_{MAX} = 0.009 (blue), α_{MAX} = 0.016 (red), and α_{MAX} = 0.16 (green). **(b)** The curves show the six $Q_P(z)$ obtained for α_{MAX} = 0.009 (blue), α_{MAX} = 0.016 (red), and α_{MAX} = 0.16 (green) with κ = 1.25e-4 m^2/s, z_0 = -1250 m (dashed), and with κ = 0.5e-4 m^2/s and z0 = -500 m (solid).

Fig. 10. Basin (solid) and plume (dashed) density as a function of depth as calculated by the numerical solution to (3.16) - (3.19), with the plume transport parameterized according to (4.25) and the entrainment function (2.5), with the velocity given by (2.4) and the bottom slope (4.26). **(a)** The curves show the solution for three different α_{MAX}; α_{MAX} = 0.009

(blue), α_{MAX} = 0.016 (red), and α_{MAX} = 0.16 (green) and two different κ and z_0; κ = 1.25e-4 m^2/s and z_0 = -1250 m (lower curves), and κ = 0.5e-4 m^2/s and z_0 = -500 m (upper curves). Also shown as thick gray lines are the non-entraining solutions (3.21) and $\Delta\rho_{CR}$ as calculated by (4.28) for α_{MAX} = 0.009 (blue), α_{MAX} = 0.016 (red), and α_{MAX} = 0.16 (green). **(b)** The curves show the six $Q_P(z)$ obtained for α_{MAX} = 0.009 (blue), α_{MAX} = 0.016 (red), and α_{MAX} = 0.16 (green) with κ = 1.25e-4 m^2/s, z_0 = -1250 m (dashed), and with κ = 0.5e-4 m^2/s and z_0 = -500 m (solid).

Fig. 11. Same as Fig. 9 but with z_0 (level of maximum bottom slope) moved to below the diffusive surface layer; namely z_0 = -2500 m (lower curves) and z_0 = -1000 m (upper curves). All other parameter values same as in Fig. 9.

Fig. 1

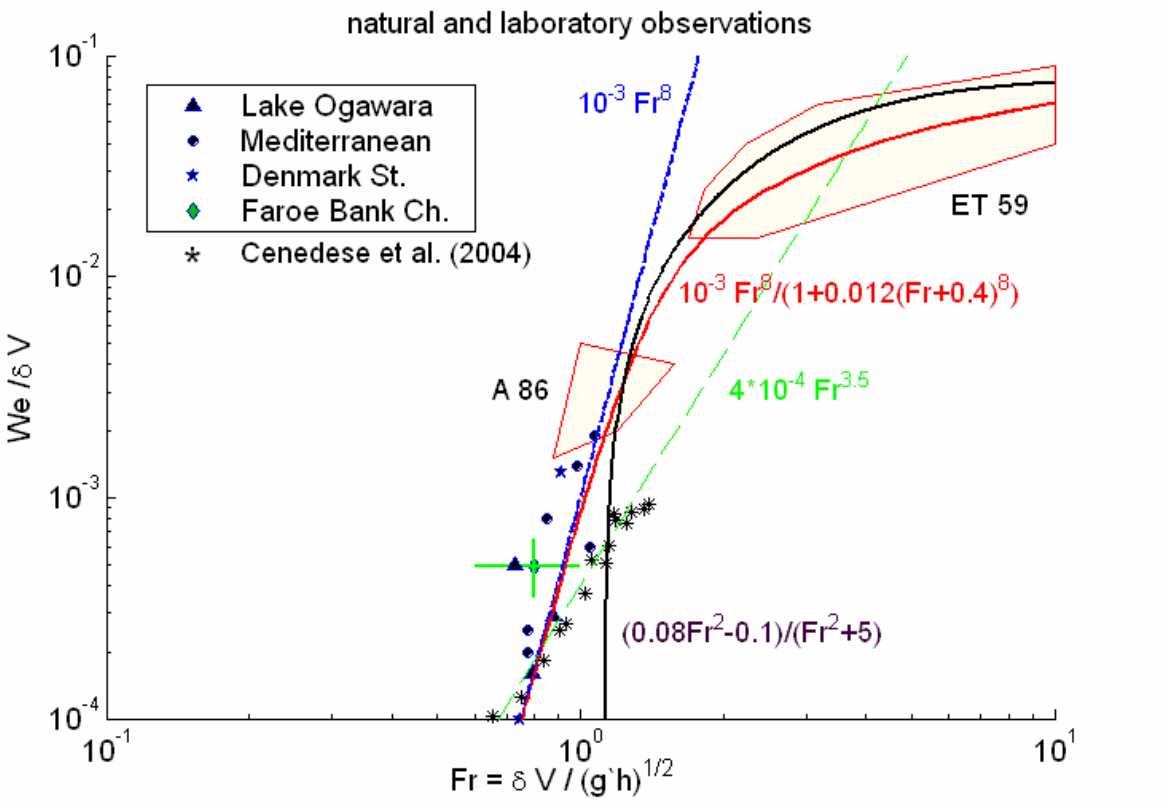
natural and laboratory observations
Lake Ogawara
Mediterranean
Denmark St.
Faroe Bank Ch.
Cenedese et al. (2004)
10-3 Fr8
ET 59
10-3 Fr8/(1+0.012(Fr+0.4)8)
A 86
4*10-4 Fr3.5
(0.08Fr2-0.1)/(Fr2+5)
We /δ V
Fr = δ V / (g`h)1/2
10-1
10-2
10-3
10-4
10-1
100
101

Fig. 2

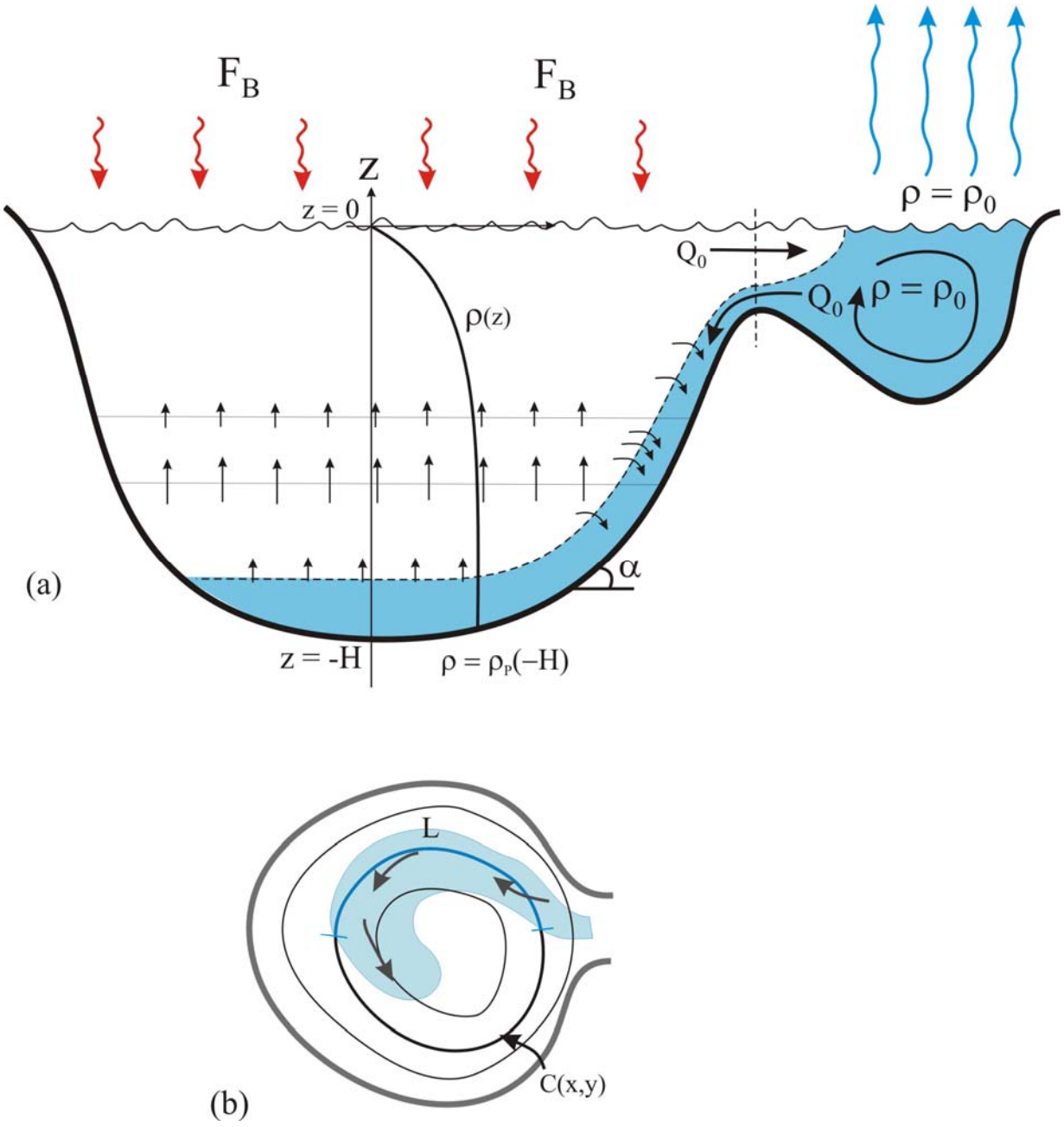

Fig. 3.

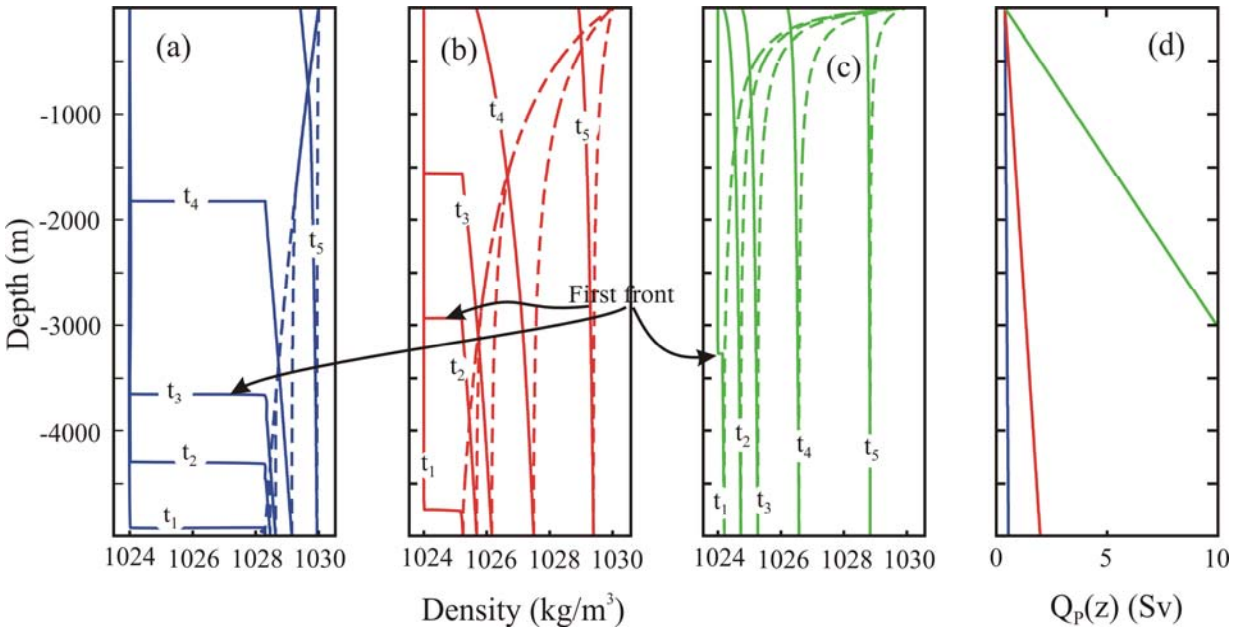
(a)
(b)
(c)
(d)
Depth (m)
-1000
-2000
-3000
-4000
t_1
t_2
t_3
t_4
t_5
First front
1024 1026 1028 1030
Density (kg/m^3)
0 5 10
$Q_p(z)$ (Sv)

Fig. 4

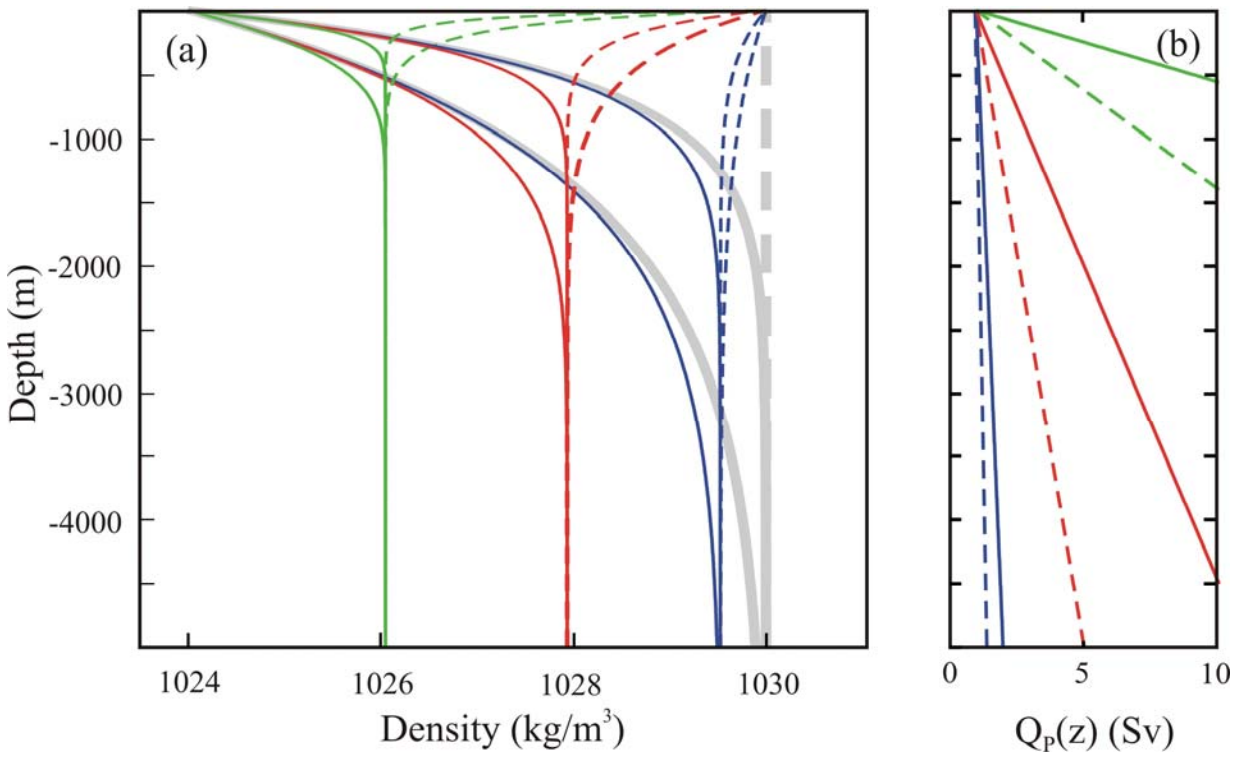
(a)
(b)
-1000
-2000
-3000
-4000
Depth (m)
1024
1026
1028
1030
Density (kg/m3)
0
5
10
QP(z) (Sv)

Fig. 5

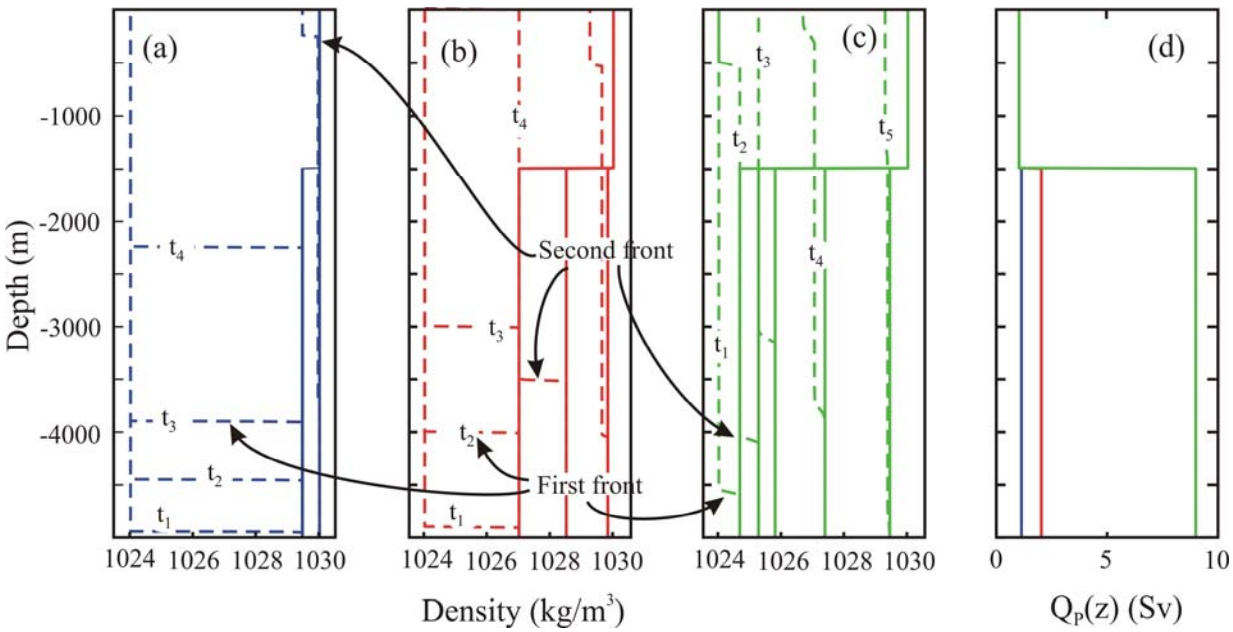
(a)
(b)
(c)
(d)
Depth (m)
-1000
-2000
-3000
-4000
t1
t2
t3
t4
t5
Second front
First front
1024 1026 1028 1030
Density (kg/m3)
0 5 10
QP(z) (Sv)

Fig. 6

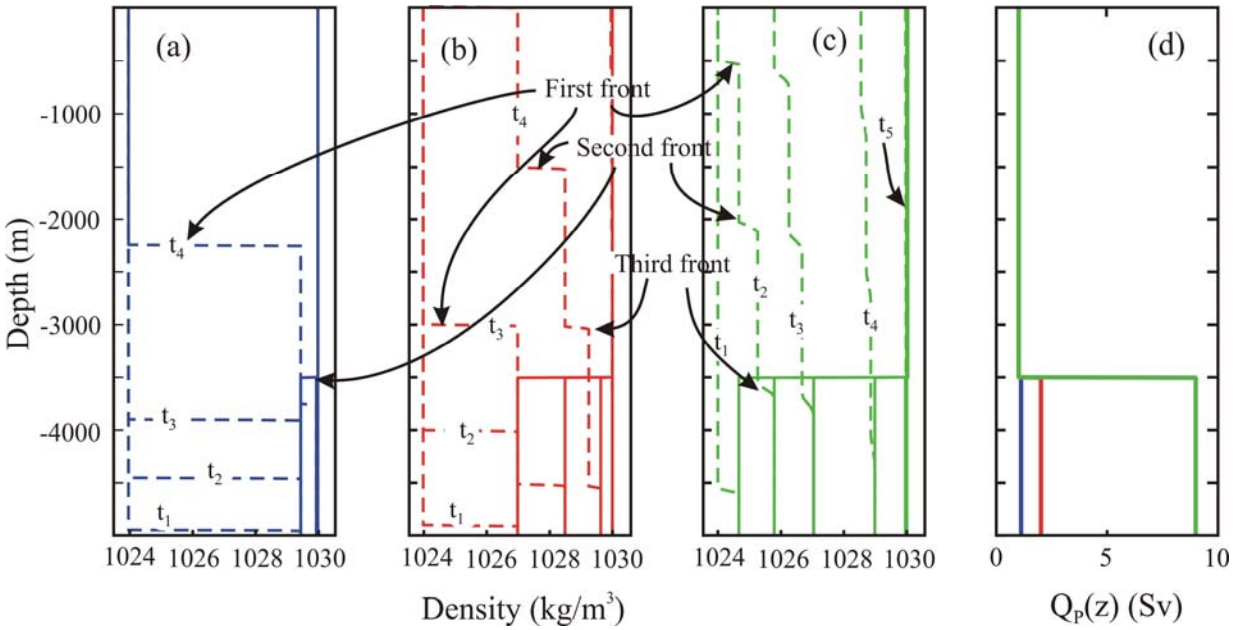
(a)
(b)
(c)
(d)
First front
Second front
Third front
Depth (m)
-1000
-2000
-3000
-4000
1024 1026 1028 1030
1024 1026 1028 1030
1024 1026 1028 1030
Density (kg/m3)
0 5 10
QP(z) (Sv)

Fig. 7

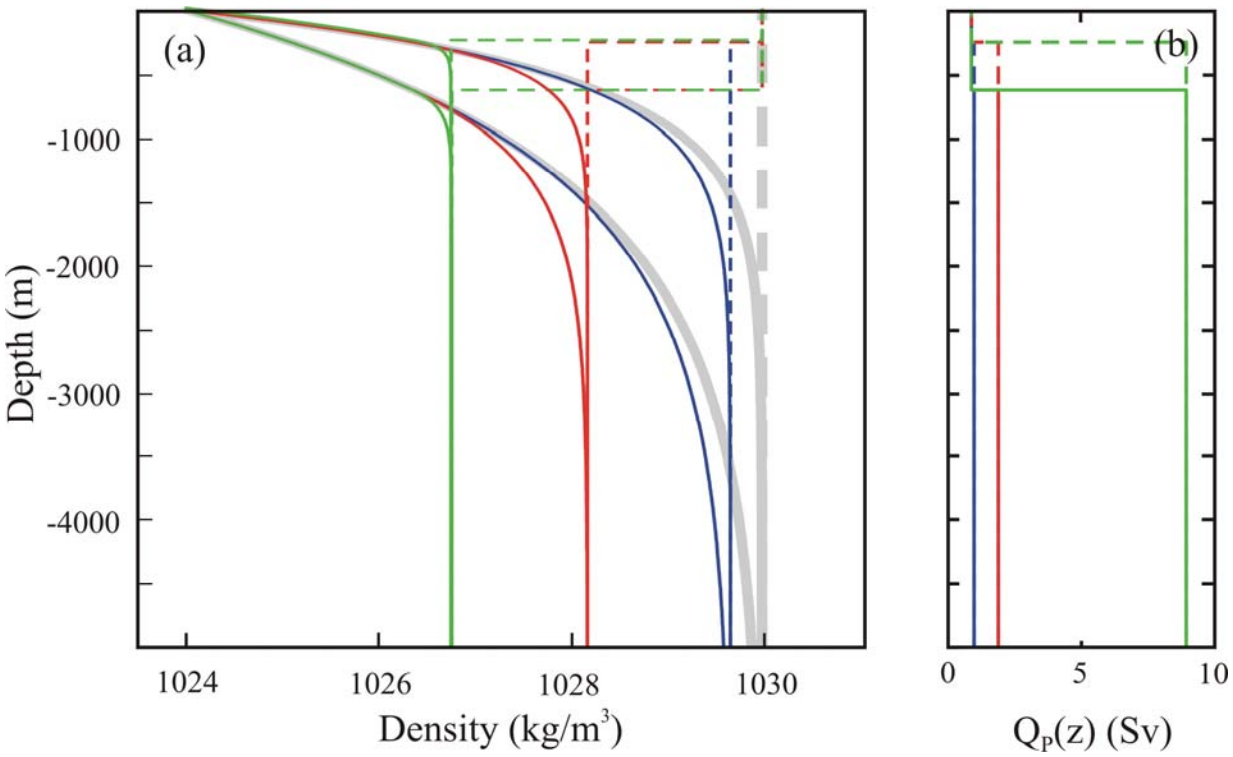
(a)
(b)
-1000
-2000
-3000
-4000
Depth (m)
1024
1026
1028
1030
Density (kg/m3)
0
5
10
QP(z) (Sv)

Fig. 8

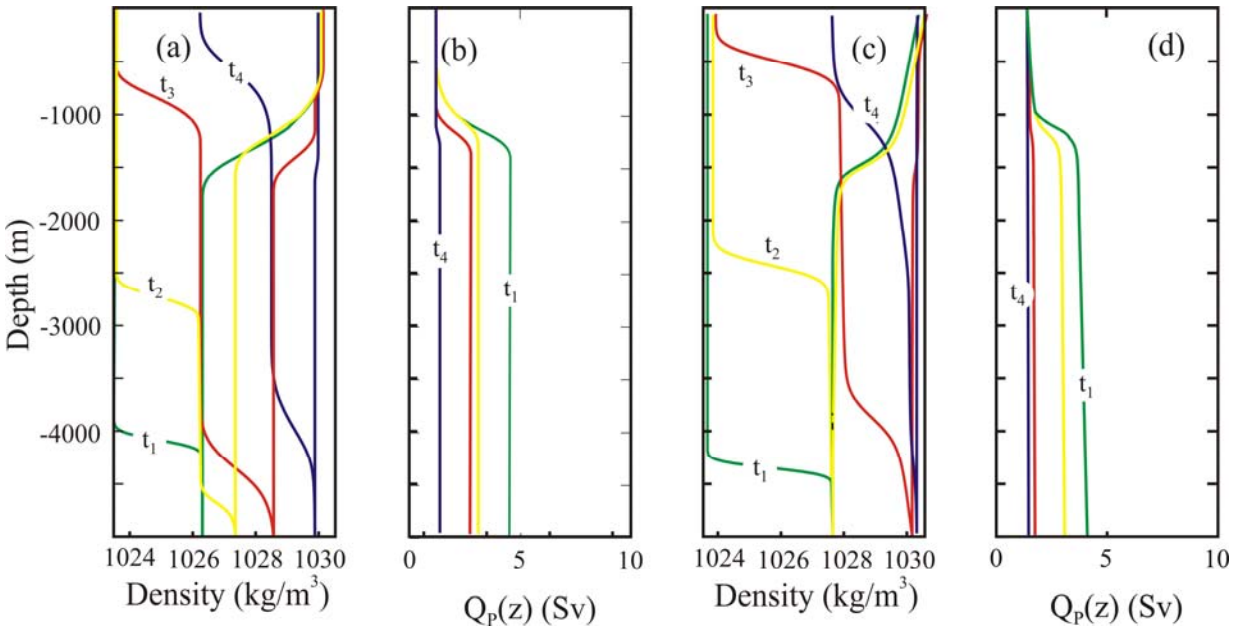
(a)
(b)
(c)
(d)
Depth (m)
-1000
-2000
-3000
-4000
t1
t2
t3
t4
1024 1026 1028 1030
Density (kg/m3)
0 5 10
Qp(z) (Sv)

Fig 9

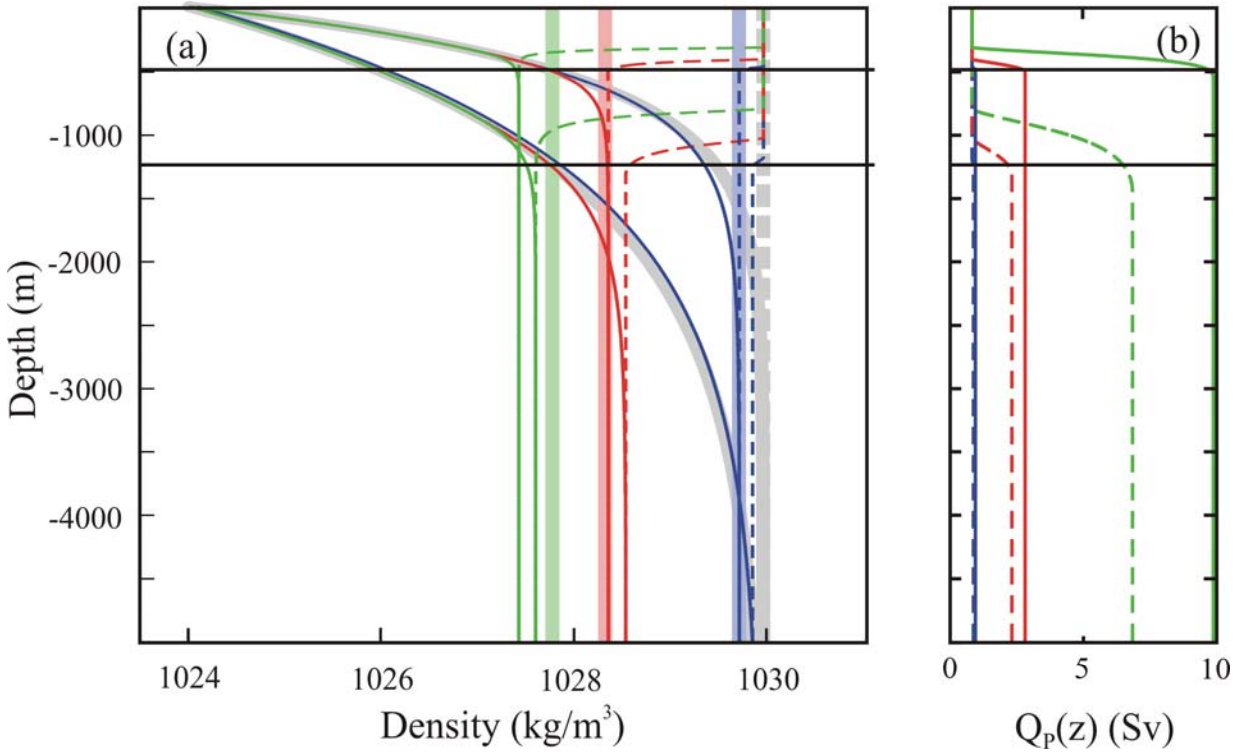
(a)
(b)
-1000
-2000
-3000
-4000
Depth (m)
1024
1026
1028
1030
Density (kg/m3)
0
5
10
QP(z) (Sv)

Fig. 10

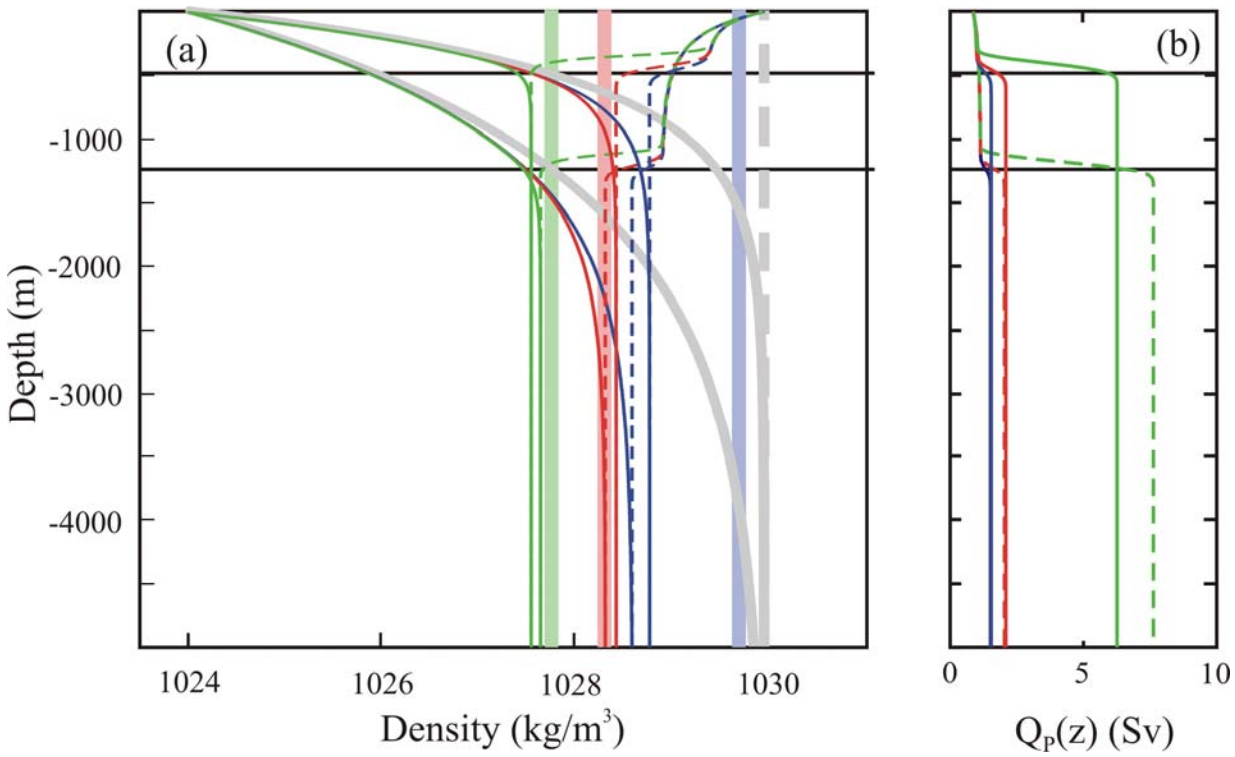
(a)
(b)
-1000
-2000
-3000
-4000
Depth (m)
1024
1026
1028
1030
Density (kg/m3)
0
5
10
QP(z) (Sv)

Fig. 11

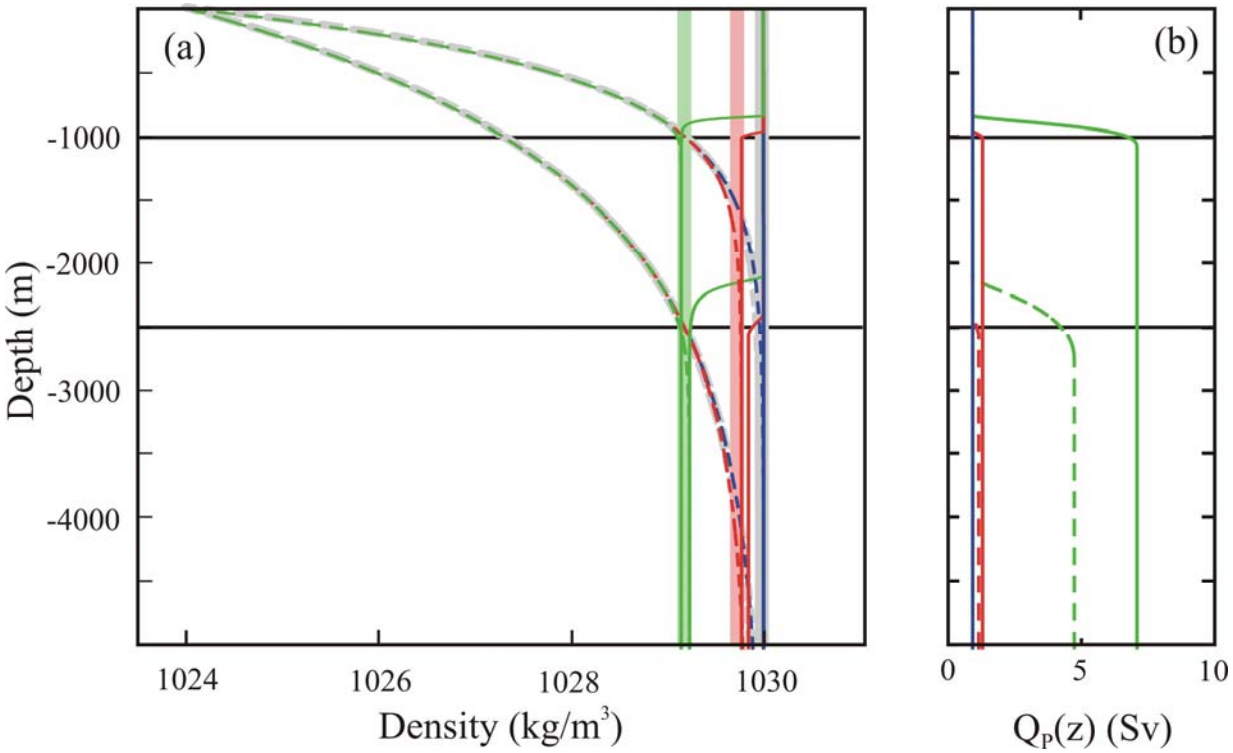
(a)
(b)
-1000
-2000
-3000
-4000
Depth (m)
1024
1026
1028
1030
Density (kg/m^3)
0
5
10
$Q_P(z)$ (Sv)